Advanced Ion Acceleration Mechanisms

S. S. Bulanov
Lawrence Berkeley National Laboratory,
Berkeley, 94720 CA, USA
sbulanov@lbl.gov

***Abstract*—One of the main applications of high power laser facilities is particle acceleration. It is due to the fact that ultrashort laser pulses in plasma are able to generate electromagnetic fields exceeding those typical for the conventional accelerators by many orders of magnitude. Laser ion acceleration is of particular interest due to unique beam properties and its potential application in basic and material science, medicine, industry, etc. There are several possible regimes where different ion acceleration mechanisms may be accessed, depending on target and laser parameters. The most well known of them is Target Normal Sheath Acceleration. However, the quest for more efficient acceleration of ion beams having different spectral features gave rise to several other advanced ion acceleration mechanisms, such as Magnetic Vortex Acceleration and Radiation Pressure Acceleration. Here the basic theoretical concepts for these advanced ion acceleration mechanisms will be presented as well as recent analytical and computer simulation results.**

I. Introduction

The laser driven acceleration of ions [**?**], [**?**], [**?**], [**?**] has recently received a lot of attention in terms of analytical, computer simulation, and experimental studies. All of them aim at optimizing laser driven ion sources for a number of potential applications, such as injectors for conventional accelerators, hadron therapy of oncological diseases, radiography, nuclear physics studies, studies of radiation damage and single event effect in electronics, as well as fast ignition inertial confinement fusion, and drivers and probes for the studies of warm dense matter. This interest is also due to the recent availability of ultrahigh power lasers [**?**], [**?**] with focused intensity up to 10^{23} W/cm^2 [**?**] and laser pulse cleaning techniques that allow a significant improvement in temporal intensity contrast enabling high intensity laser pulse interactions with a new class of ultra-thin targets. These developments gave rise to proton beams with the maximum energy just below 100 MeV from nm-scale foils of solid density [**?**], [**?**], [**?**]. While the bulk of the experimental results was obtained in the Target Normal Sheath Acceleration (TNSA) regime, higher ion energies up to several hunderd MeV or even GeV are expected to be generated by employing advanced regimes of laser ion acceleration (see, e.g., Refs. [**?**], [**?**]).

These regimes are usually characterized by more favourable scaling of the maximum ion energy with laser power. But they also require higher laser intensities and significantly better laser contrast than that required by the TNSA. The advanced regimes of laser ion acceleration include, but are not limited to, Radiation Pressure Acceleration (RPA), Coulomb Explosion (CE), and Magnetic Vortex Acceleration (MVA). Current state-of-the art computer simulations and analytical models predict that to reach several hundred MeV to GeV per nucleon maximum ion energies PW or several PW lasers are needed [**?**]. Since different laser ion acceleration regimes utilize a variety of targets and interaction setups, it is instructive to parameterize them in terms of thin foil target and extended plasma target densities (see Fig. 1). This parameterization allows to fit in one plot the regimes, which are relying on the interaction with solid density thin foils, like TNSA, RPA, and CE, and with extended plasma targets usually of near critical density (NCD), like shock wave acceleration (SWA) and MVA. Note that these densities are defined with laser intensity taken into account, i.e., high intensities make targets more transparent (see [**?**] for details).

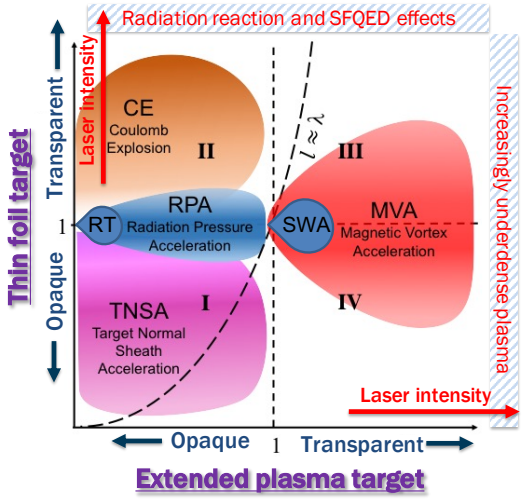

Fig. 1. The basic laser ion acceleration mechanisms parameterized in terms of thin foil target and extended plasma target densities.

The transparency thresholds marked by dashed lines in Fig. 1 subdivide the parameter space into four domains. The domains (**I**) and (**II**) correspond to thin foil targets, which are opaque or transparent for the laser respectively. Thus, the parameter domain (**I**) is mostly occupied by the TNSA regime. In the domain (**II**), the laser radiation is so intense that it

This work was supported by the U.S. Department of Energy (DOE) Office of Science, LaserNetUS, Offices of High Energy Physics and Fusion Energy Sciences under Contract No. DE- AC02–05CH11231.

is able to evacuate almost all electrons from the irradiated region of the target. The remaining ion core starts to expand rapidly, due to the repelling of noncompensated positive electric charges, i.e., it experiences Coulomb Explosion. However, more efficient laser ion acceleration regimes lie at the threshold of domains (**I**) and (**II**), where the transition from the target opacity to transparency can be utilized to optimize either the interaction volume as in the Relativistic Transparency Regime (RIT), or the energy transmission from the laser pulse to the ions as in the case of RPA.

The regions (**III**) and (**IV**) are relevant for the acceleration regimes that utilize NCD extended plasma targets, where plasma can be considered underdense for laser radiation. However being underdense does not make the target composed of such a plasma transparent. Here the target transparency is mainly determined by the laser pulse depletion. The line separating regions (**III**) and (**IV**) characterizes the targets with thicknesses equal to the depletion lengths. In such targets the laser pulse deposits almost all its energy in the plasma maximizing the energy of electrons and ions, which is crucial for the efficient operation of the SWA and MVA regimes.

Whereas almost all advanced regimes of laser ion acceleration benefit from the laser intensity increase, at some point high intensity brings in new phenomena, which make the parameterization shown in Fig. 1 invalid. That is why two boundaries are introduced in Fig. 1. The first of these boundaries states that for increasingly underdense plasma the ion acceleration mechanisms, which are mentioned in Fig. 1, cease to work. The second boundary corresponds to the threshold of the radiation reaction and strong field quantum electrodynamics (SFQED) effects. These effects for laser intensities larger than 10^{23} W/cm^2 significantly alter the process of ion acceleration (see Ref. [**?**] for details and references cited therein).

Thus, the effectiveness of the advanced regimes of laser ion acceleration depends strongly on the transparency of the target. In most cases the optimal parameters of the laser target configuration are achieved at the threshold of target transparency for thin foils and at the threshold of laser depletion for extended plasma slabs. In what follows, the two of the advanced regimes of laser ion acceleration, namely, RPA and MVA, will be reviewed with extra attention paid to the transparency/depletion effects. The paper is organized as follows. First, the RPA and factors limiting maximum attainable ion energy are described in section 2. Second, the MVA and laser depletion in NCD plasma is discussed in section 3. And, third, the modification of the MVA due to the channel target is described in section 4. The conclusions are in section 5.

II. Radiation Pressure Acceleration

The RPA has a long history, which can be traced back to conventional accelerator concepts in the 1950es, schemes for sailcraft propulsion over interstallar distances discussed as early as 1920es, and the papers by Einstein on the theory of special relativity in 1900es. From the fundamental physics point of view, the RPA is based on the relativistic receding mirror concept [**?**]. A plane electromagnetic wave reflection by a mirror moving with a relativistic velocity leads to the frequency of the reflected radiation being shifted down by a factor of $4\gamma_M^2$, where γ_M is the Lorentz factor of the mirror. This means that the energy lost by the electromagnetic wave is picked up by the mirror, which amounts to $(1-1/4\gamma_M^2)\mathcal{E}_{las}$, where $\mathcal{E}_{las}$ is the energy of the laser pulse. In the ultra-relativistic case of $\gamma_M \gg 1$ almost all laser energy is transferred to the foil. This fact is the foundation of the statement that RPA is, probably, the most effective scheme of laser ion acceleration. The following scaling of maximum ion energy, $\mathcal{E}_i$, with laser energy, $\mathcal{E}_{las}$, were obtained in Refs. [**?**], [**?**]:

$$\mathcal{E}_i = 8 \times \left(\frac{10^{11}}{N_{tot}}\right)^2 \frac{m_p}{m_i}\frac{\mathcal{E}_{las}}{1\ \mathrm{J}}\ \ \mathrm{MeV},\quad \gamma_M \ll 1, \qquad (1)$$

$$\mathcal{E}_i = 6.25 \times \frac{10^{11}}{N_{tot}}\frac{m_p}{m_i}\frac{\mathcal{E}_{las}}{100\ \mathrm{J}}\ \ \mathrm{GeV},\quad \gamma_M \gg 1, \qquad (2)$$

where N_{tot} is the total number of accelerated ions.

However, high intensity needed for RPA to happen is achieved by focusing the laser radiation in small several micron wide spots. The electromagnetic fields in this case can not be approximated by a plane electromagnetic wave. Moreover the transverse intensity profile leads to different spatial and momentum evolution of different parts of the irradiated foil. This means that the foil will deform during the interaction, which would probably make the $(1-1/4\gamma_M^2)\mathcal{E}_{las}$ scaling invalid. In what follows several effects that arise from taking into account more realistic features of the laser target interaction in the RPA regime are discussed (see Ref. [**?**] for details).

These effects include sub-luminal laser group velocity, laser off-normal incidence, target transparency, and transverse target expansion (see Fig. 2). Taking into account the sub-luminal laser group velocity, leads to the ion energy gain being proportional to the difference between the instantaneous foil velocity and the laser group velocity $\Delta\mathcal{E} \approx 2\gamma^2\beta(\beta-\beta_g)\mathcal{E}_{las}$. Thus, the RPA can not produce ions with the velocity exceeding the laser group velocity. If the laser off-normal incidence is used, this imposes another limit on maximum attainable ion energy, because the component of the laser group velocity perpendicular to the foil surface is further limited by the cosine of the incidence angle. Target transparency is probably the most severe limiting effect, because the RPA effectiveness is mainly determined by the amount of laser radiation that is being reflected by the foil, any radiation that is transmitted does not participate in the acceleration. The transverse target expansion is closely connected with the target transparency effect. Due to the transverse intensity profile of the laser pulse, different parts of the irradiated area acquire different velocities, which leads to the target deformation during the interaction and transverse expansion. This means that the target density starts to decrease and the effectiveness of acceleration also goes down. Thus, the concept of laser transparency plays the central role in analysing the effectiveness of RPA.

Recently, several concepts to compensate for the these limiting factors were proposed.

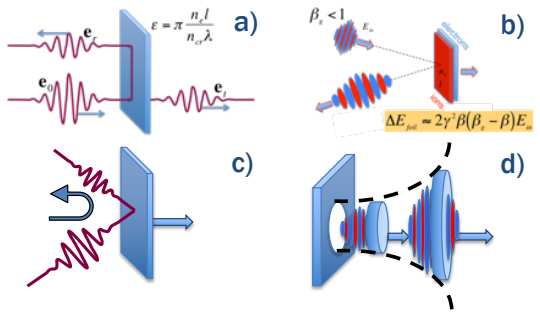

Fig. 2. The factors limiting maximum attaianable ion energy in RPA: target transparency (a), laser group velocity (b), off-normal incidence (c), and target transverse expansion (d).

In what follows it is shown how the effects of the sub-luminal laser group velocity, target transparency, and transverse target expansion can be taken into account in the framework of a simple analytical model for the acceleration of an on-axis element of the foil. Since RPA usually requires high laser intensities, laser pulses tightly focused to a small focal spot, w_0, need to be utilized. In this case the laser group velocity is smaller than the vacuum light speed, $\beta_g \simeq 1 - 1/k^2 w_0^2$, where k is the amplitude of the laser wavevector. Small w_0 means that the Raleigh length of such a pulse is only several wavelengths, $L_R = \pi w_0^2/\lambda$, where λ is the wavelength of the laser. The laser field depends on the distance from the focus as $a(x) = a_0/\sqrt{1+(x/L_R)^2}$, where a_0 is the laser field amplitude at focus and x is the coordinate along which the laser propagates. If one assumes that the target expansion follows the laser pulse profile as it diverges from focal plane, then the target surface density, $n_e l$, decrease is inversely proportional to the laser waist increase squared:

$$w(x) = w_0\sqrt{1+(x/L_R)^2}, \tag{3}$$

$$n_e l = n_0 l_0 \left[1+(x/L_R)^2\right]^{-1}. \tag{4}$$

Here n_e and l are density and thickness of the target, and n_0 and l_0 are initial density and thickness of the target. In this case the transparency parameter ε_p scales as $\varepsilon_p(x) = \varepsilon_p(0)\left[1+(x/L_R)^2\right]^{-1}$ with the distance from focus. Using these expressions one can write the equation of motion for the expanding foil under the action of a diverging laser pulse:

$$\frac{d\beta}{dt} = |\rho(x)|^2 \frac{m_e}{m_i}\frac{a^2(\psi)}{\varepsilon_p}\beta_g(1-\beta^2)^{1/2}(\beta_g-\beta)(1-\beta\beta_g). \tag{5}$$

There are several important features in the right-hand-side of this equation corresponding to the limiting factors mentioned above. First, it is proportional to the difference between the instantaneous ion velocity and the laser group velocity. Second, the density decrease is compensated by the field amplitude decrease, but the effect of the transverse expansion also modifies the reflection coefficient, since only it depends on the coordinate x.

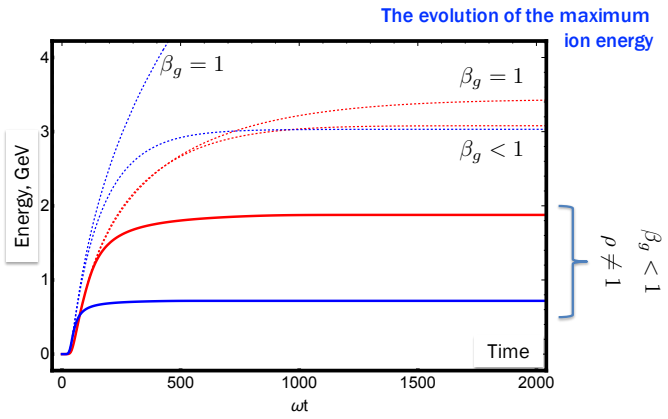

Fig. 3. The evolution of the maximum ion energy for two laser f-numbers: f/D=1 (blue curves) and f/D=2 (red curves). The curves are marked according to the limiting factors taken into account. The upper dashed curves with $\beta_g = 1$ correspond to the group velocity equal to the speed of light, the target being opaque, and no transverse expansion is present. The dashed curves with $\beta_g < 1$ are obtained taking into account the laser group velocity being smaller than the speed of light. The solid curves take into account all three limiting factors.

The results of the solution of this equation can be seen in Fig. 3, where the evolution of the maximum ion energy for two laser f-numbers (f/D=1 and f/D=2) is shown. The laser pulse is 1.8 PW and 30 fs duration, the foil is 0.25λ thick and its density is 400 n_{cr}, where $n_{\rm cr} = m_e\omega^2/(4\pi e^2)$ is the plasma critical density, e and m_e are the charge and mass of an electron respectively. The solid lines represent the solutions with sub-luminal laser group velocity, target transparency, and transverse target expansion taken into account. Note, that the temporal profile of the laser pulse is Gaussian in all the considered cases, while the RPA operation can be enhanced by employing temporatl profile tailoring by matching the target transparency to the instantaneous field strength. From this point of view Gaussian profiles are not optimal for RPA, since the target might become transparent during the interaction, thus, reducing the effectiveness of acceleration. The dashed lines are illustrating the significance of the limiting factors when comparing to the idealised RPA with 100% reflection and plane wave modeling the laser. Note that the transverse expansion is the most limiting factor of all taken into account. It can also be seen from comparing the f/D=1 and f/D=2 cases. The stronger is the focusing of the laser pulse, the stronger is the transverse expansion since it follows the laser divergence.

Several concepts were proposed on how to compensate for these limiting factors. Most of them were suggesting to modify the target, by either shaping it or by employing composite targets (see, e.g., Refs. [**?**], [**?**], [**?**], [**?**]. However, hybrid acceleration schemes, which would use RPA at early stages of acceleration were also proposed, as well as the RPA modification with laser shaping.

III. Magnetic Vortex Acceleration

The magnetic vortex acceleration scheme relies on the high intensity laser being able to creates a low density channel

in the extended plasma target. As the laser propagates in this self created channel it drives a strong electron current along the propagation direction. This current generates strong magnetic field, which, upon the laser exiting from the backside of the target, generates strong charge separation electric field, which can both accelerate and focus the ions (see Fig. 4 and Fig. 5). In order to quantify this acceleration mechanism the waveguide model can be employed [**?**], which describes the properties of the laser field inside the channel based on the solution of the wave equation in the cylindrical waveguide. In the framework of this model the dimensionless vector potential and radius of the self-generated channel (waveguide) are

$$a_{\rm ch} = \left(\frac{2}{K}\frac{P}{P_c}\frac{n_e}{n_{\rm cr}}\right)^{1/3}, \quad R_{\rm ch} = \frac{\lambda}{\pi}\left(\frac{n_{\rm cr}}{n_e}\right)^{1/3}\left(\frac{2}{K}\frac{P}{P_c}\right)^{1/6}. \tag{6}$$

where $K = 1/13.5$ is the geometrical factor, P is the laser power, n_e is the initial electron density in the target, and $P_c = 2m_e^2c^5/e^2 = 17\text{GW}$ is a characteristic power for relativistic self-focusing. Note that the radius of the channel is determined from balancing the energy gain of an electron in a laser field and in the field of an ion column.

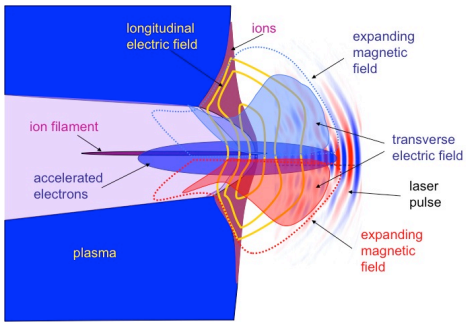

Fig. 4. The scheme of the MVA, showing the distributions of electron and ion densities overlaid with the electric and magnetic field distributions.

As it was mentioned above the optimal conditions for the ion acceleration via MVA are determined at the threshold of laser depletion in the NCD plasma. Since the laser energy is mostly transferred to electrons via the ponderomotive scattering, the depletion length can be obtained by balancing the laser energy inside the channel, W_p, and the energy of electrons, W_e, which interacted with the laser. It is assumed that on average the electron energy gain is $m_ec^2a_{\rm ch}$. Then for a laser pulse with given power, P, length, $L_p = c\tau$ (τ is the laser pulse duration), the density of plasma depends on the depletion length as

$$\frac{n_e}{n_{\rm cr}} = 2^{1/2}K\left(\frac{P}{P_c}\right)^{1/2}\left(\frac{L_p}{L_{\rm ch}}\right)^{3/2}. \tag{7}$$

This equation shows that for a specific plasma density the target thickness should be chosen appropriately to achieve maximum acceleration.

Let us next estimate the fields generated by the laser pulse propagation in the self-generated channel [**?**]. The electrons accelerated in the wake of the laser pulse form a thin filament

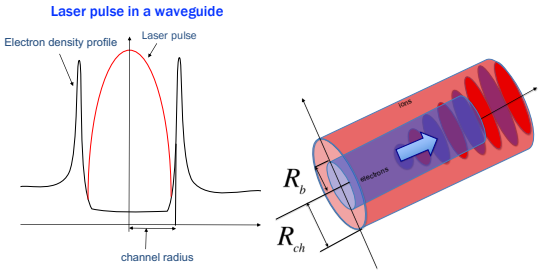

Fig. 5. The schematic representation of laser pulse propagation in the self-created plasma channel. The pinching of the electron current due to the plasma lens effect.

along the central axis. They carry a strong electric current, which is due to the plasma lensing effect. One can estimate the radiaus of the electron current by balancing the the self field of an electron beam and the transverse electric field of the ion column: $R_{\rm b} = R_{\rm ch}/\gamma_e$ (see Fig. 5b). The Lorentz factor γ_e is that of the bulk of electrons accelerated forward. It is plausible to assume that the velocity of these electrons is of the order of the laser group velocity in a waveguide of radius $R_{\rm ch}$: $\gamma_e = (\sqrt{2}/1.84)(2P/KP_c)^{1/6}(n_{\rm cr}/n_e)^{1/3}$.

The maximum strength of the magnetic field is reached at $r = R_{\rm b}$ scales with the laser pulse power as

$$B_{\rm ch} = 2\pi e\left(\frac{\lambda}{\pi}\right)n_{\rm cr}\left(\frac{\sqrt{2}}{1.84}\right)^2\left(\frac{2}{K}\frac{P}{P_c}\right)^{1/2}. \tag{8}$$

Note that the magnetic field strength scales as the square root of laser power.

As the laser exits the target from the back, this magnetic field displaces the electron component of the plasma with respect to the ion one. This leads to the electric field generation, roughly of the same order of magnitude, which accelerates and collimates ions in the form of a well defined beam with achromatic divergence [**?**], [**?**]. These accelerated ions mainly originate from the same filamentary structure, since the electron current pre-accelerates a number of ions as it propagates through the ion channel. The energy of ions according to the analytical estimate scales with laser power as $\mathcal{E} \sim P^{4/3}$ in the case of ion motion being non-relativistic and as $\mathcal{E} \sim P^{2/3}$ in the relativistic case. The scalings for the magnetic field strength and maximum ion energy are corroborated by three-dimensional computer simulations [**?**], [**?**].

IV. Laser Ion Shotgun Acceleration

Though the RPA demonstrate high efficiency of laser energy transformation into the energy of accelerated ions and the MVA demonstrate the generation of a collimated well defined ion beam, the resulting potential ion sources do not meet the requirements of most applications. These requirements do not only include ion energy but also energy spread and total beam charge. Most laser ion acceleration mechanisms find it challenging to meet all the requirements, especially, when the ion energy exceeds 100 MeV per nucleon.

It can be shown how a laser ion acceleration mechanism that generates a broad spectrum with a monotonically decreasing number of energetic particles can be modified to produce a mono-energetic peak [**?**]. Here an MVA-type acceleration is followed by the creation of a dense forward-moving electron bunch which is enabled by a structured target, which is a channel with solid density walls pre-filled with an NCD plasma and a strong plasma magnetic field. Before the formation of this bunch the accelerated ions has a typical MVA distribution with a positive chirp, which means that the ion energy increases along the direction of laser pulse propagation. The structured target enables strong focusing of the electron current at the exit from the channel. This bunch generates a strong positive longitudinal and transversely focusing electric field. Then this field starts to modify the ion distribution by compensating the chirp, i. e., by accelerating the lower energy ions and reducing the divergence of the ions. As a result a 2 PW, 120 fs laser can produce a quasi-monoenergetic peak centered at 230 MeV. The number of protons in a 40 MeV energy interval around this peak is about 5×10^{10} (7.8 nC). Thus, the target engineering can modify the well-known ion acceleration mechanisms leading to the production of accelerated ion beams with properties required by applications.

V. Conclusions

The results on different mechanisms of laser driven ion acceleration clearly indicate the the advanced ion acceleration mechanisms are needed to accelerate ions to energies exceeding 100 MeV/u. Here two of these mechanisms were reviewed, Radiation Pressure Acceleration and Magnetic Vortex Acceleration, since the former demonstrates the highest energy transformation efficiency, while the latter produces a collimated ion beam with a high total charge.

The analytical and computer simulation studies show that the concepts of target transparency in the RPA case and laser depletion in the MVA case play the central role in analyzing the efficiency of advanced ion acceleration mechanisms. While the optimal RPA can be defined as the acceleration of an opaque to radiation thin foil, where the opaqueness is achieved by a minimum possible number of ions, the optimal MVA is defined as almost 100% depletion of laser energy in NCD plasma, but the laser is still able to penetrate the target.

It was shown that the optimization of acceleration mechanisms is needed to overcome different limiting factors and generate ion beams with required for application properties. For RPA and MVA this can be achieved by utilizing the composite targets, as well as the laser pulse and target shaping. Moreover, recent experimental results from the PW-class laser facilities are very encouraging from the point of view of reaching energies more that 100 MeV and exploring the parameter space of advanced ion acceleration mechanisms. For example, the commissioning of the BELLA PW iP2 beamline [**?**] up to 17 J of energy has demonstrated a focused proton beam with high charge and up to 40 MeV energy [**?**].

Acknowledgment

I would like to acknowledge the contribution of my co-authors to the joint papers on advanced ion acceleration mechanisms, which were reviewed here: C. Benedetti, A. J. Gonsalves, S. Hakimi, J. DeChant, M. Garten, C. G. R. Geddes, A. Huebl, K. Nakamura, L. Obst-Huebl, C. B. Schroeder, J. van Tilborg, Cs. Toth, M. Turner, J.-L. Vay, and E. Esarey from Lawrence Berkeley National Laboratory, S. V. Bulanov and G. Korn from ELI Beamlines, T. Zh. Esirkepov, J. K. Koga, K. Kondo, and M. Kando from National Institutes for Quantum and Radiological Science and Technology, F. Pegararo from the University of Pisa, T. Toncian from Helmholtz Zentrum Dresden Rossendorf, and A. V. Arefiev and Z. Gong from the University of California, San Diego.

References

[1] G. Mourou, T. Tajima, and S. V. Bulanov, Rev. Mod. Phys. **78**, 309 (2006).

[2] H. Daido, M. Nishiuchi, and A. S. Pirozhkov, Reports on Progress in Physics **75**, 056401 (2012).

[3] A. Macchi, M. Borghesi, and M. Passoni, Rev. Mod. Phys. **85**, 751 (2013).

[4] S. V. Bulanov, Ja. J. Wilkens, T. Zh. Esirkepov, et. al., Phys. Usp. **57**, 1149 (2014).

[5] C. N. Danson, C. Haefner, J. Bromage, T. Butcher, J.-C. F. Chanteloup, E. A. Chowdhury, *el. al.*, High Power Laser Science and Engineering 7, e54 (2019).

[6] A. Gonoskov, T. Blackburn, M. Marklund, S. S. Bulanov, Rev. Mod. Phys. 94, 045001 (2022).

[7] J. W. Yoon, Y. G. Kim, I. Choi, J. H. Sung, H. W. Lee, S. K. Lee, and C. H. Nam, Optica 8 (5), 630 (2021).

[8] I. J. Kim, K. H. Pae, C. M. Kim, C.-L. Lee, I. W. Choi, H. T. Kim, *el. al.*, Phys. Plasmas 23, 070701 (2016).

[9] F. Wagner, O. Deppert, C. Brabetz, P. Fiala, A. KleinSchmidt, P. Poth, *el. al.*, Phys. Rev. Lett. 116, 205002 (2016).

[10] A. Higginson, R. J. Gray, M. King, R. J. Dance, S. D. R. Williamson, N. M. H. Butler, *el. al.*, Nat. Commun. 9, 724 (2018).

[11] S. S. Bulanov, E. Esarey, C. B. Schroeder, S. V. Bulanov, T. Z. Esirkepov, M. Kando, F. Pegoraro, and W. P. Leemans, Phys. Plasmas 23 (5), 056703 (2016).

[12] S. V. Bulanov, T. Zh. Esirkepov, M. Kando, A. S. Pirozhkov, and N. N. Rosanov, Phys. Usp. 56, 429 (2013).

[13] O. Klimo, J. Psikal, J. Limpouch, and V. T. Tikhonchuk, Phys. Rev. ST Accel. Beams 11, 031301 (2008).

[14] S. V. Bulanov, T. Zh. Esirkepov, F. Pegoraro, and M. Borghesi, Comp. Rendus Physique 10, 216 (2009).

[15] S. V. Bulanov, E. Yu. Echkina, T. Zh. Esirkepov, I. N. Inovenkov, M. Kando, F. Pegoraro, and G. Korn, Phys. Rev. Lett. 104, 135003 (2010).

[16] J. H. Bin, W. J. Ma, H. Y. Wang, M. J. V. Streeter, C. Kreuzer, D. Kiefer, *el. al.*, Phys. Rev. Lett. 115, 064801 (2015)

[17] S. S. Bulanov, E. Esarey, C. B. Schroeder, S. V. Bulanov, T. Zh. Esirkepov, M. Kando, F. Pegoraro, and W. P. Leemans, Phys. Rev. Lett. 114, 105003 (2015).

[18] T. Wang, V. Khudik, and G. Shvets Phys. Rev. Lett. 126, 024801 (2021).

[19] S. S. Bulanov, V. Yu. Bychenkov, V. Chvykov, G. Kalinchenko, D. W. Litzenberg, T. Matsuoka, A. G. R. Thomas, L. Willingale, V. Yanovsky, K. Krushelnick, and A. Maksimchuk, Phys. Plasmas 17, 043105 (2010).

[20] S. S. Bulanov, E. Esarey, C. B. Schroeder, W. P. Leemans, S. V. Bulanov, D. Margarone, G. Korn, and T. Haberer, Phys. Rev. Spec. Top. - Accel. Beams 18, 061302 (2015).

[21] J. Park, S. S. Bulanov, J. Bin, Q. Ji, S. Steinke, J-L. Vay, Phys. Plasmas 26, 103108 (2019).

[22] S. Hakimi, L. Obst-Huebl, A. Huebl, K. Nakamura, S. S. Bulanov, S. Steinke, *el. al.*, Phys. Plasmas 29, 083102 (2022).

[23] Z. Gong, S. S. Bulanov, T. Toncian, A. Arefiev, Phys. Rev. Res. 4, L042031 (2022).

[24] S. Hakimi, L. Obst-Huebl, K. Nakamura, A. Huebl, S. S. Bulanov, A. Jewell, *el. al.*, in this Proceedings – submitted.